GPCR-dependent biasing of GIRK channel signaling dynamics by RGS6 in mouse sinoatrial nodal cells

Allison Anderson[a], Ikuo Masuho[b], Ezequiel Marron Fernandez de Velasco[a], Atsushi Nakano[c], Lutz Birnbaumer[d,e], Kirill A. Martemyanov[b], and Kevin Wickman[a,1]

[a]Department of Pharmacology, University of Minnesota, Minneapolis, MN 55455; [b]Department of Neuroscience, The Scripps Research Institute, Jupiter, FL 33458; [c]Department of Molecular, Cell, and Developmental Biology, University of California, Los Angeles, CA 90095; [d]Neurobiology Laboratory, National Institute of Environmental Health Sciences, Research Triangle Park, NC 27709; and [e]Biomedical Research Institute, Catholic University of Argentina, C1107AAZ Buenos Aires, Argentina

Edited by David E. Clapham, Howard Hughes Medical Institute Janelia Research Campus, Ashburn, VA, and approved May 1, 2020 (received for review January 22, 2020)

How G protein-coupled receptors (GPCRs) evoke specific biological outcomes while utilizing a limited array of G proteins and effectors is poorly understood, particularly in native cell systems. Here, we examined signaling evoked by muscarinic (M_2R) and adenosine (A_1R) receptor activation in the mouse sinoatrial node (SAN), the cardiac pacemaker. M_2R and A_1R activate a shared pool of cardiac G protein-gated inwardly rectifying K^+ (GIRK) channels in SAN cells from adult mice, but A_1R-GIRK responses are smaller and slower than M_2R-GIRK responses. Recordings from mice lacking Regulator of G protein Signaling 6 (RGS6) revealed that RGS6 exerts a GPCR-dependent influence on GIRK-dependent signaling in SAN cells, suppressing M_2R-GIRK coupling efficiency and kinetics and A_1R-GIRK signaling amplitude. Fast kinetic bioluminescence resonance energy transfer assays in transfected HEK cells showed that RGS6 prefers $G\alpha_o$ over $G\alpha_i$ as a substrate for its catalytic activity and that M_2R signals preferentially via $G\alpha_o$, while A_1R does not discriminate between inhibitory G protein isoforms. The impact of atrial/SAN-selective ablation of $G\alpha_o$ or $G\alpha_{i2}$ was consistent with these findings. $G\alpha_{i2}$ ablation had minimal impact on M_2R-GIRK and A_1R-GIRK signaling in SAN cells. In contrast, $G\alpha_o$ ablation decreased the amplitude and slowed the kinetics of M_2R-GIRK responses, while enhancing the sensitivity and prolonging the deactivation rate of A_1R-GIRK signaling. Collectively, our data show that differences in GPCR-G protein coupling preferences, and the $G\alpha_o$ substrate preference of RGS6, shape A_1R- and M_2R-GIRK signaling dynamics in mouse SAN cells.

muscarinic | adenosine | Kir3 | G protein | heart rate

G protein-coupled receptors (GPCRs) constitute the largest family of cell-surface receptors in the mammalian genome, and they mediate the influence of a diverse array of ligands on cell signaling, organ physiology, and behavior (1). GPCRs evoke biological responses by coupling to a limited array of heterotrimeric G proteins, which then regulate the activity of a relatively small pool of effectors. Mechanisms underlying the compartmentalization of G protein-dependent signaling pathways in native cell types are not well understood.

Regulation of heart rate (HR) offers an opportunity to investigate how different GPCRs engage intracellular signaling networks to shape a critical physiological response. Activation of the parasympathetic branch of the autonomic nervous system elicits bradycardia (2), an effect mediated by the acetylcholine (ACh)-induced activation of M_2 muscarinic receptors (M_2R) on sinoatrial nodal (SAN) cells (3). M_2R activation stimulates inhibitory G proteins, which then modulate the activity of downstream effectors, including the G protein-gated inwardly rectifying K^+ (GIRK) channel (4–6). The cardiac GIRK channel is a heterotetramer consisting of GIRK1 and GIRK4 subunits (7–9). Studies involving *Girk1*$^{-/-}$ and *Girk4*$^{-/-}$ mice have shown that activation of cardiac GIRK channels mediates most of the parasympathetic impact on HR, as well as atrial and atrioventricular (AV) impulse conduction (10–13). Cardiac GIRK channels are also activated by adenosine (Ado), an autacoid generated under ischemic conditions that activates the A_1 adenosine receptor (A_1R), resulting in GIRK-dependent bradycardia (10, 14–16). The ability of Ado to suppress HR and AV impulse conduction is exploited clinically to treat and diagnose supraventricular tachycardias (14).

GPCR-dependent signaling dynamics are influenced by Regulator of G protein Signaling (RGS) proteins (17). RGS proteins possess GTPase-activating protein (GAP) catalytic activity that accelerates the intrinsic GTP hydrolysis rate of G protein alpha (Gα) subunits. Previous work from our group and others has identified RGS6 as a critical negative regulator of M_2R-GIRK signaling in mouse SAN cells and atrial myocytes (18–20). RGS6 is a member of the R7 RGS subfamily of RGS proteins, members of which form obligate dimers with the atypical Gβ subunit Gβ5 (21). Genetic ablation of *Rgs6* in mice increased GIRK channel sensitivity to muscarinic receptor activation, prolonged the deactivation rate of currents elicited by the nonselective cholinergic agonist carbachol (CCh), and enhanced CCh-induced bradycardia (18–20). The extent to which RGS6 regulates A_1R-GIRK signaling in the heart is currently unknown.

Here, we probed the functional compartmentalization of GPCR-dependent signaling by investigating signaling engaged by M_2R and A_1R activation in SAN cells. Despite converging on a common effector, M_2R-GIRK and A_1R-GIRK signaling pathways

Significance

Mechanisms promoting the compartmentalization of G-protein signaling are poorly understood in native cells. This study examined muscarinic (M_2R) and adenosine (A_1R) receptor signaling to a common effector—the G protein-gated inwardly rectifying K^+ (GIRK) channel—in mouse sino-atrial nodal (SAN) cells. Regulator of G protein Signaling 6 (RGS6) exerts a GPCR-dependent influence on the efficacy, kinetics, and sensitivity of GIRK-dependent signaling in SAN cells, suppressing M_2R-GIRK signaling kinetics and sensitivity and A_1R-GIRK signaling amplitude. The distinctions can be explained by the differential utilization of G protein isoforms by M_2R and A_1R and a $G\alpha_o$ substrate preference of RGS6. Thus, GPCR-G protein signaling and RGS-G protein substrate biases shape GIRK-dependent signaling dynamics in the mouse heart.

Author contributions: A.A., K.A.M., and K.W. designed research; A.A., I.M., and E.M.F.d.V. performed research; I.M., A.N., L.B., and K.A.M. contributed new reagents/analytic tools; A.A., I.M., E.M.F.d.V., and K.W. analyzed data; and A.A., I.M., A.N., L.B., K.A.M., and K.W. wrote the paper.

The authors declare no competing interest.

This article is a PNAS Direct Submission.

[1]To whom correspondence may be addressed. Email: wickm002@umn.edu.

This article contains supporting information online at https://www.pnas.org/lookup/suppl/doi:10.1073/pnas.2001270117/-/DCSupplemental.

First published June 8, 2020.

display notable differences in amplitude and kinetics. Using an array of knockout mouse lines, as well as electrophysiological, molecular, and optical imaging approaches, we found that the differences in M_2R-GIRK and A_1R-GIRK signaling dynamics in mouse SAN cells can be explained by GPCR-specific coupling biases for inhibitory G protein isoforms and the $G\alpha_o$ substrate specificity of RGS6.

Results

A_1R-GIRK and M_2R-GIRK Signaling Distinctions in Mouse SAN Cells. We began by measuring whole-cell currents evoked by a saturating concentration of either Ado (10 μM) or CCh (10 μM) in isolated SAN cells from C57BL/6J (wild-type) mice (Fig. 1). Both agonists reliably evoked currents in SAN cells from wild-type mice, but not in SAN cells from congenic *Girk4*$^{-/-}$ mice (Fig. 1 *A* and *B*), indicating that the evoked responses were mediated by GIRK channel activation. Currents elicited by Ado in wild-type SAN cells were smaller than CCh-induced currents (Fig. 1*C*) and did not exhibit acute desensitization (Fig. 1*D*). In addition, activation and deactivation rates of Ado-induced GIRK currents were slower than those of CCh-induced responses (Fig. 1 *E* and *F*).

RGS6 Exerts a GPCR-Dependent Influence on GIRK-Dependent Signaling. In parallel, we explored the impact of *Rgs6* ablation on Ado- and CCh-induced currents in SAN cells. While Ado-induced currents were significantly larger in SAN cells from *Rgs6*$^{-/-}$ mice relative to wild-type controls (Fig. 1 *A* and *C*), there was no impact of *Rgs6* ablation on CCh-induced current amplitudes (Fig. 1 *B* and *C*). *Rgs6* ablation also exerted a GPCR-dependent impact on response kinetics. Loss of RGS6 correlated with prolonged activation rate of Ado-induced currents (Fig. 1*E*), but there was no impact on deactivation rate (Fig. 1*F*). In contrast, and consistent with published reports (18, 19), there was no impact of *Rgs6* ablation on the activation rate of CCh-induced currents (Fig. 1*F*), but deactivation rate was prolonged (Fig. 1*F*). Acute desensitization of CCh- and Ado-induced currents was not impacted by *Rgs6* ablation (Fig. 1*D*). Thus, RGS6 normally suppresses the amplitude and accelerates the activation rate of A_1R-GIRK signaling in mouse SAN cells, while accelerating the deactivation rate of M_2R-GIRK signaling.

Ado-induced currents in SAN cells from *Rgs6*$^{-/-}$ mice were completely reversed by the GIRK channel inhibitor rTertiapin-Q (TTQ, 300 nM; *SI Appendix*, Fig. S1) (22, 23), indicating that the enhanced Ado-induced responses in these cells involves an increase in GIRK-dependent signaling. There was no difference in GIRK1, GIRK4, or A_1R mRNA levels in atrial tissue samples containing the SAN region from wild-type and *Rgs6*$^{-/-}$ mice (*SI Appendix*, Fig. S2). Additionally, GIRK channel currents evoked by ML297, a direct and selective activator of GIRK1-containing GIRK channels (24, 25), were modestly but significantly smaller in SAN cells from *Rgs6*$^{-/-}$ mice (*SI Appendix*, Fig. S3). Thus, the increase in Ado-induced GIRK currents in SAN cells from *Rgs6*$^{-/-}$ mice does not appear to be linked to an increase in the expression of A_1R or GIRK channels.

To address the impact of *Rgs6* ablation on the sensitivity of M_2R-GIRK and A_1R-GIRK signaling pathways, we measured GIRK currents evoked by increasing concentrations of Ado and CCh in SAN cells from wild-type and *Rgs6*$^{-/-}$ mice. While there was no impact of *Rgs6* ablation on the sensitivity of GIRK channels to Ado (Fig. 2 *A*–*C*), GIRK channels in SAN cells from *Rgs6*$^{-/-}$ mice were more sensitive to CCh than GIRK channels in SAN cells from wild-type controls (Fig. 2 *D*–*F*) (19). Thus, RGS6

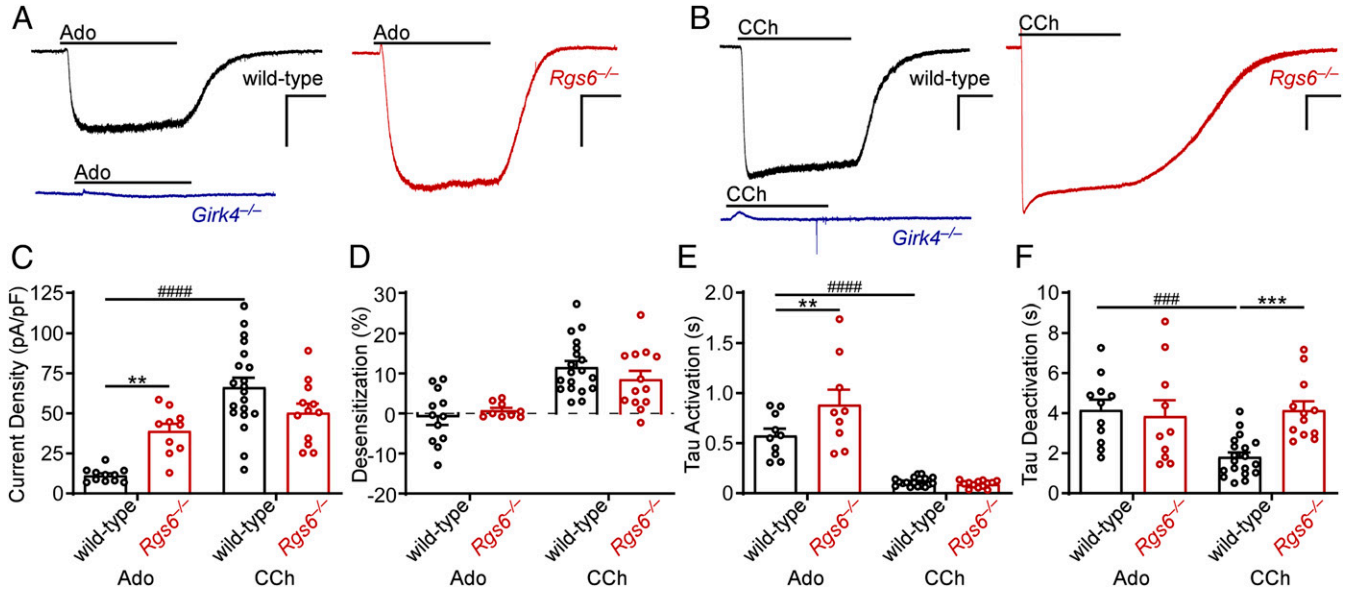

Fig. 1. Ado- and CCh-induced GIRK currents in SAN cells. (*A* and *B*) Whole-cell currents (V_{hold} = −70 mV) evoked by Ado (10 μM; *A*) or CCh (10 μM; *B*) in SAN cells from wild-type (*Left*, black) and *Rgs6*$^{-/-}$ (*Right*, red) mice; these currents were not observed in SAN cells from *Girk4*$^{-/-}$ mice (*Bottom*, blue). (Scale bars: 5 s/500 pA.) (*C*) Peak current density of responses elicited by Ado (*Left*) and CCh (*Right*) in SAN cells from wild-type (black) and *Rgs6*$^{-/-}$ (red) mice. There was a significant interaction between genotype and agonist ($F_{1,49}$ = 14.9, P < 0.001; two-way ANOVA); group sizes ranged from 10 to 20 cells (5–7 mice). **P < 0.01 wild-type vs. *Rgs6*$^{-/-}$ (within agonist); ####P < 0.0001 Ado vs. CCh (wild-type). (*D*) Acute desensitization of responses elicited by Ado (*Left*) and CCh (*Right*) in SAN cells from wild-type (black) and *Rgs6*$^{-/-}$ (red) mice. Statistical analysis revealed a main effect of agonist ($F_{1,49}$ = 30.4, P < 0.0001; two-way ANOVA), but no main effect of genotype ($F_{1,49}$ = 0.13, P = 0.72; two-way ANOVA) or genotype x agonist interaction ($F_{1,49}$ = 1.6, P = 0.21; two-way ANOVA); group sizes ranged from 9 to 19 cells (5–7 mice). (*E*) Activation rates of responses elicited by Ado (*Left*) and CCh (*Right*) in SAN cells from wild-type (black) and *Rgs6*$^{-/-}$ (red) mice. Statistical analysis revealed a genotype x agonist interaction ($F_{1,45}$ = 6.8, P < 0.05; two-way ANOVA); group sizes ranged from 9 to 17 cells (5–7 mice). **P < 0.01 wild-type vs. *Rgs6*$^{-/-}$ (within agonist); ####P < 0.0001 Ado vs. CCh (wild type). (*F*) Deactivation rates of responses elicited by Ado (*Left*) and CCh (*Right*) in SAN cells from wild-type (black) and *Rgs6*$^{-/-}$ (red) mice. Statistical analysis revealed a genotype x agonist interaction ($F_{1,48}$ = 8.0, P < 0.01; two-way ANOVA); group sizes ranged from 12 to 19 cells (5–7 mice). ***P < 0.001 wild-type vs. *Rgs6*$^{-/-}$ (within agonist); ###P < 0.001 Ado vs. CCh (wild type).

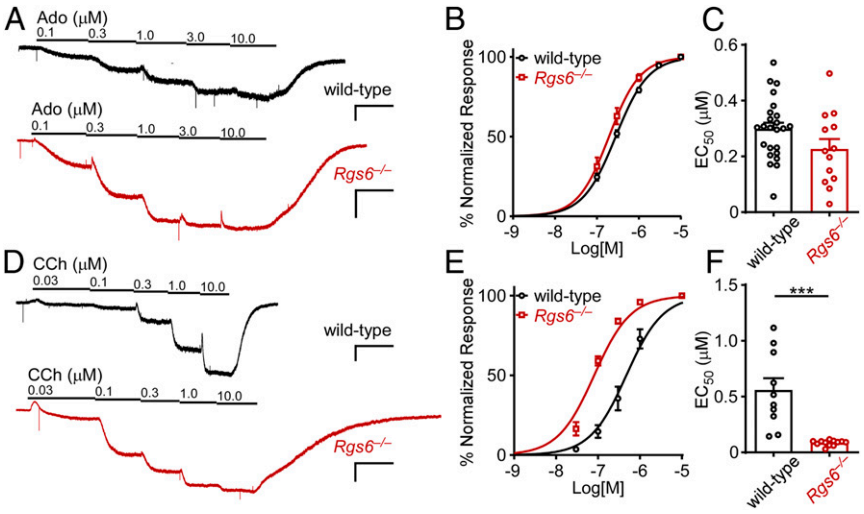

Fig. 2. Impact of *Rgs6* ablation on GIRK channel sensitivity to CCh and Ado. (*A*) Concentration-response experiments for Ado in SAN cells from wild-type (Scale bars: *Top*, 10 s/200 pA.) and *Rgs6*$^{-/-}$ (Scale bars: *Bottom*, 10 s/500 pA.) mice. (*B* and *C*) Summary of concentration-response experiments for Ado-induced currents in SAN cells from wild-type and *Rgs6*$^{-/-}$ mice. There was no difference in EC_{50} values for Ado-induced currents in SAN cells from wild-type (n = 24 cells/7 mice) and *Rgs6*$^{-/-}$ (n = 13 cells/5 mice) mice (t_{35} = 1.8, P = 0.08; unpaired t test). (*D*) Concentration-response experiments for CCh-induced currents in SAN cells from wild-type (Scale bars: *Top*, 10 s/200 pA.) and *Rgs6*$^{-/-}$ (*Scale bars: *Bottom*, 10 s/500 pA.) mice. (*E* and *F*) Summary of concentration-response experiments of CCh-induced currents in SAN cells from wild-type and *Rgs6*$^{-/-}$ mice. The EC_{50} values for CCh-induced currents in SAN cells from *Rgs6*$^{-/-}$ (n = 12 cells/4 mice) mice were lower than the EC_{50} values measured in wild-type counterparts (n = 10 cells/4 mice) (t_{20} = 4.8, ***P < 0.001; unpaired t test).

decreases GIRK channel sensitivity to CCh, but not Ado, in SAN cells.

RGS6 Impacts GIRK-Dependent Bradycardia in a GPCR-Dependent Manner. We also evaluated the impact of *Rgs6* ablation on the bradycardic effect of A_1R and M_2R activation using an isolated heart model (Fig. 3). Both the stable A_1R agonist N6-cyclopentyl-adenosine (CPA) (Fig. 3 *A* and *B*) and CCh (Fig. 3 *C* and *D*) evoked dose-dependent decreases in HR in wild-type hearts. The bradycardic effect of CPA and CCh was strongly diminished in hearts from *Girk4*$^{-/-}$ mice (Fig. 3 *B* and *D*), suggesting that M_2R- and A_1R-induced bradycardia is largely dependent on GIRK channel activation. The magnitude of CPA-induced bradycardia was larger in *Rgs6*$^{-/-}$ as compared to wild-type hearts (Fig. 3*B*), but there was no detectable shift in CPA potency. While CCh-induced bradycardia was also more pronounced in *Rgs6*$^{-/-}$ hearts (18, 19, 26), there was a clear leftward shift in the dose–response curve (Fig. 3*D*). Thus, the results from the isolated heart model mirror the results obtained from isolated SAN cells, indicating that RGS6 exerts a prominent negative influence on A_1R-GIRK signaling amplitude and M_2R-GIRK signaling sensitivity.

RGS6 Limits the Access of A_1R to GIRK Channels. The differential impact of *Rgs6* ablation on M_2R-GIRK and A_1R-GIRK signaling in mouse SAN cells could reflect the coupling of the GPCRs to separate pools of GIRK channels. To test this possibility, we examined whether Ado-induced currents were occluded by a maximal CCh-induced GIRK channel response. In both wild-type and *Rgs6*$^{-/-}$ SAN cells, Ado failed to evoke an additive

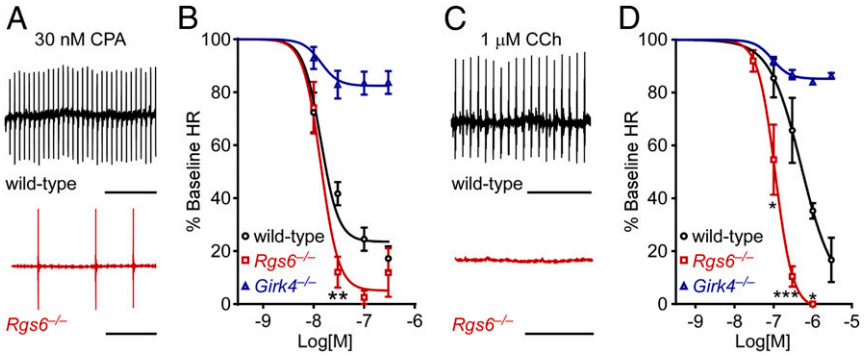

Fig. 3. CPA- and CCh-induced bradycardia in isolated hearts from wild-type and *Rgs6*$^{-/-}$ mice. (*A*) Segments of ECG traces from isolated wild-type (*Top*) and *Rgs6*$^{-/-}$ (*Bottom*) hearts perfused with the A_1R-selective agonist CPA (30 nM). (Scale bar: 5 s.) (*B*) Percentage decrease in HR (relative to baseline) following perfusion of increasing concentrations of CPA in hearts from wild-type (n = 6), *Rgs6*$^{-/-}$ (n = 7), and *Girk4*$^{-/-}$ (n = 4) mice; there was a genotype x CPA concentration interaction for wild-type and *Rgs6*$^{-/-}$ hearts ($F_{4,44}$ = 2.81; P < 0.05; two-way ANOVA with repeated measures). **P < 0.01 wild type vs. *Rgs6*$^{-/-}$. (*C*) Segments of ECG traces of isolated wild-type (*Top*) and *Rgs6*$^{-/-}$ (*Bottom*) hearts perfused with CCh (1 μM). (Scale bar: 5 s.) (*D*) Percentage decrease in HR (relative to baseline) following perfusion of increasing concentrations of CCh in hearts from wild-type (n = 3), *Rgs6*$^{-/-}$ (n = 5), and *Girk4*$^{-/-}$ (n = 6) mice; there was a genotype x CCh concentration interaction for wild-type and *Rgs6*$^{-/-}$ hearts ($F_{3,18}$ = 5.1, P < 0.05; two-way ANOVA with repeated measures). *P < 0.05 and ***0.001, respectively, wild type vs. *Rgs6*$^{-/-}$.

current during application of a saturating concentration of CCh (Fig. 4 *A* and *B*). When the order of agonist application was reversed, CCh evoked an additive current during the Ado-induced response (Fig. 4*C*). The size of the CCh-induced additive response was substantially smaller, however, in SAN cells from *Rgs6*$^{-/-}$ mice (Fig. 4*D*). Indeed, the Ado-induced GIRK current occluded nearly all of the CCh-induced response. Collectively, these findings show that M_2R and A_1R couple to a shared pool of GIRK channels in SAN cells and that RGS6 effectively limits the access of A_1R to GIRK channels in these cells.

M_2R and A_1R Display Overlapping but Distinct G Protein Coupling Preferences. We next investigated whether the utilization of different Gα isoforms by M_2R and A_1R could explain the differences in GIRK channel-dependent signaling and modulation by RGS6. Treatment with pertussis toxin abolished CCh- and Ado-induced currents in wild-type SAN cells (*SI Appendix*, Fig. S4), indicating that M_2R– and A_1R-GIRK signaling pathways are mediated by inhibitory ($G_{i/o}$) G proteins. To probe the inhibitory G protein coupling preferences for M_2R and A_1R, we employed a Bioluminescence Resonance Energy Transfer (BRET) assay to measure G protein activation in response to GPCR stimulation in living cells (Fig. 5*A*) (27).

We quantified maximal BRET response amplitudes and G protein activation rates for M_2R and A_1R in the presence of specific G protein isoforms (Fig. 5*B*). Analysis of BRET amplitudes showed that both M_2R and A_1R can activate all members of the $G_{i/o}$ subfamily, as well as G_{15} (Fig. 5*C*). M_2R displayed faster activation rates with $G\alpha_o$ relative to $G\alpha_i$ isoforms, however, while A_1R exhibited similar activation rates for $G\alpha_o$ and $G\alpha_i$ isoforms (Fig. 5*D*). Since G protein activation rates closely reflect the catalytic activity of GPCRs (28), whereas amplitudes in the BRET assay could be influenced by intrinsic differences in the extent of heterotrimer dissociation (29), we relied on activation rate as a proxy for Gα coupling preferences for M_2R and A_1R. Accordingly, M_2R exhibits a coupling preference for $G\alpha_o$ over $G\alpha_i$, whereas A_1R does not discriminate between the inhibitory G protein isoforms.

$G\alpha_o$ Is the Preferred Substrate for RGS6 GAP Activity. Given the distinct G protein isoform coupling preferences displayed by M_2R and A_1R, and the differential impact of RGS6 on G protein-mediated regulation of GIRK channels, we next tested whether the RGS6 exhibits a G protein isoform preference for its catalytic activity. The G protein deactivation rates of all $G\alpha_{i/o}$ members were measured in the presence of RGS6/Gβ5 using a modified version of the BRET assay (Fig. 6*A*). The D_2 dopamine receptor (D_2R), dopamine, and haloperidol were chosen for this study due to previous work showing that D_2R can efficiently activate all $G\alpha_{i/o}$ G proteins and that GTPase activity is the rate-limiting step in response deactivation for this combination of receptor and ligands (28). Consistent with results from a study involving purified RGS6/Gβ5 and G proteins (30), RGS6/Gβ5 strongly accelerated the deactivation of $G\alpha_{oA/B}$, while showing only weak activity toward $G\alpha_{i1\text{-}3}$ isoforms and no activity toward $G\alpha_z$ (Fig. 6 *B* and *C*). Thus, $G\alpha_o$ is the preferred substrate for RGS6 and its GAP activity.

$G\alpha_o$ and $G\alpha_{i2}$ Ablation Impact GIRK-Dependent Signaling in a GPCR-Dependent Manner. Previous work utilizing constitutive or conditional knockout mice has implicated $G\alpha_o$ and $G\alpha_{i2}$ isoforms in HR regulation (31–33). Accordingly, we crossed an atrial-specific Cre driver line (SLNCre) (34) with conditional $G\alpha_o$ ($G\alpha_o^{fl/fl}$) (35) or $G\alpha_{i2}$ ($G\alpha_{i2}^{fl/fl}$) (32) knockout mice to generate mice lacking $G\alpha_o$ (SLNCre:$G\alpha_o^{fl/fl}$) or $G\alpha_{i2}$ (SLNCre:$G\alpha_{i2}^{fl/fl}$) in atrial (including SAN) tissue. We then recorded currents evoked by CCh or Ado in SAN cells from Cre(+) and Cre(−) littermates (Fig. 7). While maximal CCh-induced currents and desensitization were smaller in SLNCre(+):$G\alpha_o^{fl/fl}$ SAN cells compared to Cre(−) littermates (Fig. 7 *A*–*C*), Ado-induced currents and desensitization were not impacted by $G\alpha_o$ ablation (Fig. 7 *F*–*H*). $G\alpha_{i2}$ ablation had no impact on CCh- or Ado-induced response amplitudes or desensitization (Fig. 7 *B*, *C*, *G*, and *H*). Loss of $G\alpha_o$ prolonged activation and deactivation rates of CCh-induced GIRK currents, whereas $G\alpha_{i2}$ ablation was without effect (Fig. 7 *D* and *E*). The deactivation rate of Ado-induced GIRK currents was also prolonged by $G\alpha_o$ ablation (Fig. 7*J*), but

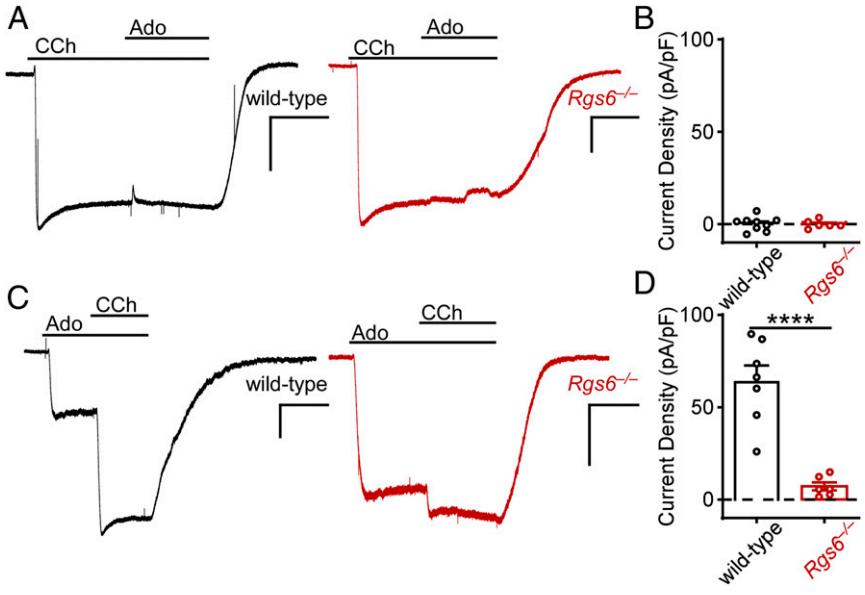

Fig. 4. Occlusion of CCh- and Ado-induced GIRK currents. (*A*) Occlusion experiments showing whole-cell currents elicited by a maximal concentration of CCh (10 μM), followed by Ado application (10 μM) in SAN cells from wild-type (*Left*) and *Rgs6*$^{-/-}$ (*Right*) mice. (Scale bars: 10 s/500 pA.) (*B*) There was no difference in the Ado-induced additive response in SAN cells isolated from wild-type ($n = 9$ cells/4 mice) and *Rgs6*$^{-/-}$ ($n = 6$ cells/5 mice) mice ($t_{13} = 0.11$, $P = 0.91$; unpaired *t* test). (*C*) Occlusion experiments showing whole-cell currents elicited by a maximal concentration of Ado (10 μM), followed by CCh application (10 μM) in SAN cells from wild-type (*Left*) and *Rgs6*$^{-/-}$ (*Right*) mice. (Scale bars: 10 s/500 pA.) (*D*) There was a significant difference in the CCh-induced additive response in SAN cells from wild-type ($n = 7$ cells/4 mice) and *Rgs6*$^{-/-}$ ($n = 6$ cells/4 mice) mice ($t_{11} = 6.0$; ****$P < 0.0001$; unpaired *t* test).

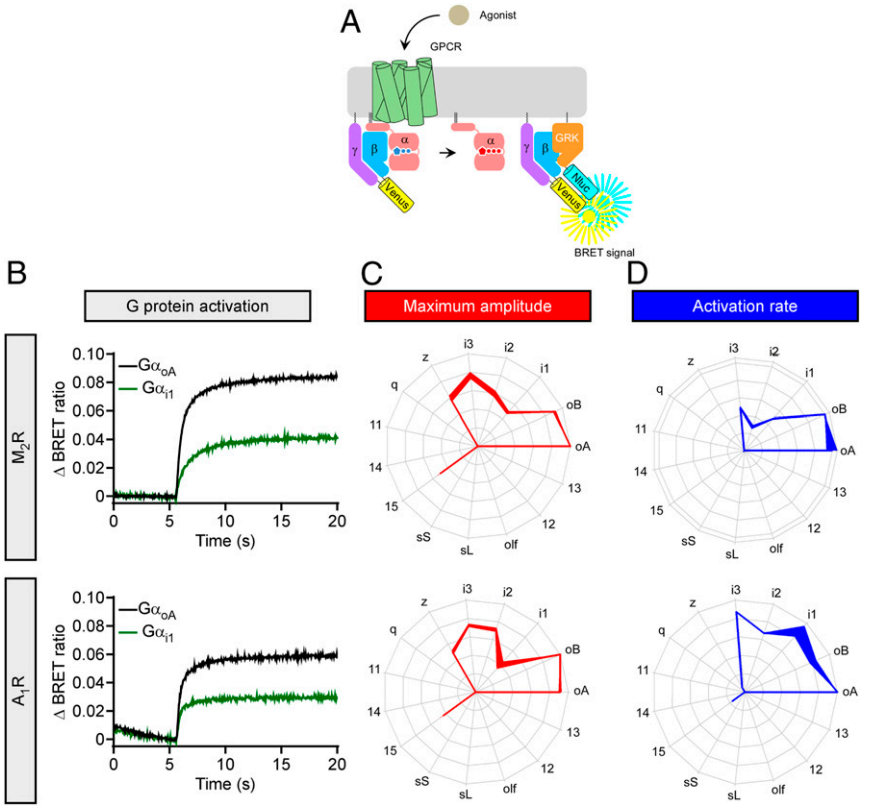

Fig. 5. G protein coupling preferences of M_2R and A_1R. (*A*) Schematic representation of the BRET assay for real-time optical imaging of G protein activity. Agonist-induced activation of a GPCR leads to the dissociation of Gα-GTP and Venus-Gβγ subunits. The released Venus-Gβγ then interacts with the Gβγ effector mimetic masGRK3ct-Nluc-HA to produce the BRET signal. (*B*) Representative real-time monitoring of G protein activation by M_2R (*Top*) or A_1R (*Bottom*). HEK293T/17 cells were transfected with the BRET sensor pair (*A*) and GPCR, together with either $G\alpha_{oA}$ (black) or $G\alpha_{i1}$ (green). Acetylcholine (100 μM) or Ado (100 μM) was applied at the 5-s time point, and the BRET signal was followed across time. (*C* and *D*) G protein coupling summary diagrams for M_2R and A_1R. Maximum amplitudes (red) and activation rate constants (blue) for 15 different G proteins were normalized to the largest value and plotted in the wheel diagrams. Line thickness represents the SEM of three technical replicates performed independently.

interestingly, the activation rate of Ado-induced GIRK currents was accelerated by $G\alpha_{i2}$ ablation (Fig. 7*I*). Collectively, these results align with observations that M_2R signals preferentially through $G\alpha_o$, whereas A_1R does not discriminate between $G\alpha_o$ and $G\alpha_i$. Moreover, the lack of impact of $G\alpha_{i2}$ ablation on the CCh- and Ado-induced GIRK current deactivation rates is consistent with the $G\alpha_o$ substrate preference of RGS6.

Finally, we evaluated the impact of $G\alpha_o$ or $G\alpha_{i2}$ ablation on GIRK channel sensitivity to CCh and Ado. While the loss of $G\alpha_o$ did not impact GIRK channel sensitivity to CCh (Fig. 8 *A–C*), $G\alpha_{i2}$ ablation increased the sensitivity of GIRK channels to CCh. Conversely, $G\alpha_o$ ablation increased GIRK channel sensitivity to Ado, whereas $G\alpha_{i2}$ ablation was without effect (Fig. 8 *D–F*). Thus, loss of $G\alpha_o$ increases the sensitivity of A_1R-GIRK channel signaling, whereas loss of $G\alpha_{i2}$ increases the sensitivity of M_2R-GIRK channel signaling.

Discussion

While M_2R and A_1R signal to a shared pool of GIRK channels in mouse SAN cells, the amplitude and kinetics of these signaling pathways are distinct. RGS6 exerts a GPCR-dependent influence on GIRK-dependent signaling in mouse SAN cells, modulating the sensitivity and kinetics of M_2R-GIRK signaling and the amplitude of A_1R-GIRK signaling. Innate GPCR-G protein coupling preferences appear to contribute to the distinctions in M_2R- and A_1R-GIRK signaling pathways in SAN cells. Our data suggest that $G\alpha_o$ plays a more important role in mediating M_2R-GIRK than A_1R-GIRK signaling in mouse SAN cells. This, together with the strong $G\alpha_o$ substrate preference of RGS6, provides a plausible explanation for the GPCR-dependent influence of RGS6 on GIRK-dependent signaling in mouse SAN cells.

A_1R-GIRK responses are smaller than M_2R-GIRK responses in mouse SAN cells; parallel observations have been noted in mouse, rat, and guinea pig atrial myocytes (36–38). A maximal M_2R-induced GIRK response completely occludes the A_1R-GIRK response in SAN cells, suggesting that M_2R activation can elicit a maximal GIRK-dependent response, while A_1R activation can engage only a fraction of available GIRK channels. Different levels of M_2R and A_1R expression likely contribute to the differences in response amplitudes and activation kinetics. Indeed, overexpression of A_1R in rat atrial myocytes increased Ado-induced GIRK currents and accelerated the current activation rate (39). Thus, the level of A_1R and/or G protein intermediate appears to limit A_1R-GIRK signaling amplitude in mouse SAN cells.

Considering the GAP activity of RGS6, *Rgs6* ablation should result in increased steady-state levels of activated $G\alpha_o$ (and Gβγ) following M_2R and A_1R activation. Indeed, A_1R-GIRK response amplitudes were enhanced by *Rgs6* ablation without upregulation of A_1R or GIRK channels. Thus, the amplitude of A_1R-GIRK signaling in mouse SAN cells is likely limited by the amount of activated G protein released by A_1R activation. Interestingly, loss of RGS6 had no impact on CCh-induced GIRK current amplitude, suggesting that the GIRK channel limits the

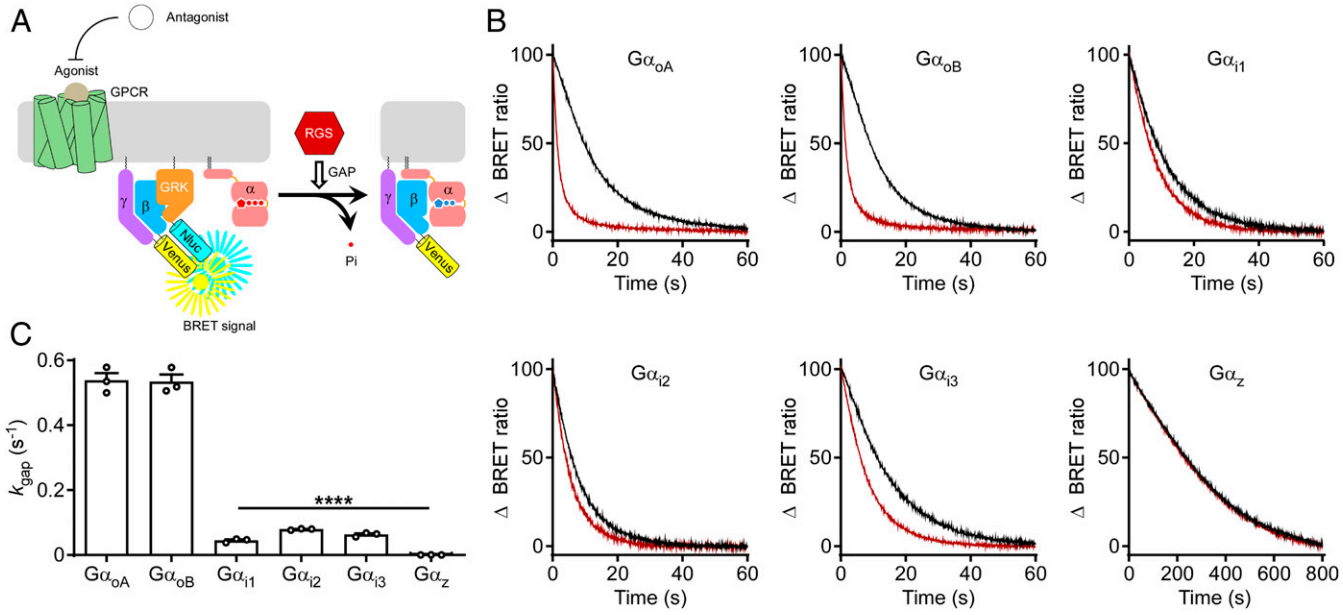

Fig. 6. Gα substrate specificity of RGS6/Gβ5. (*A*) Schematic representation of the BRET assay for measuring RGS GAP activity. Application of antagonist after G protein activation by a GPCR agonist initiates the deactivation of G proteins, decreasing the BRET signal. (*B*) Real-time monitoring of G protein deactivation. HEK293T/17 cells were transfected with D_2R, Gα, Venus-Gβγ, and masGRK3ct-Nluc-HA with (red) or without (black) RGS6/Gβ5. Dopamine (100 μM) and haloperidol (100 μM) were applied to activate D_2R and initiate G protein deactivation, respectively. Representative data from three independent experiments are shown. (*C*) Comparison of kGAP activity of RGS6/Gβ5 on the $G_{i/o}$ isoforms ($F_{5,12} = 372.6$, $P < 0.0001$; one-way ANOVA). ****$P < 0.0001$ vs. $G\alpha_o$ isoforms.

M_2R-GIRK responses in these cells, a contention supported by our occlusion data. The enhanced sensitivity of GIRK channels to CCh in SAN cells from *Rgs6*$^{-/-}$ mice further suggests that the loss of RGS6 effectively increases the fraction of spare M_2R receptors in these cells. Interestingly, we recently reported an increase in M_2R-GIRK current amplitude in ventricular myocytes from *Rgs6*$^{-/-}$ mice, where expression M_2R is lower than in the atria (40). Thus, RGS6 may impact GPCR-effector response amplitudes when the level of G protein, rather than effector, is limiting.

RGS proteins may also facilitate GIRK-dependent signaling in a GAP-independent manner. Mice heterozygous for an RGS-insensitive $G\alpha_o$, for example, exhibit blunted GIRK channel responses to mu opioid receptor (MOR) activation in some neurons (41), suggesting that RGS proteins promote MOR-GIRK coupling. Notably, we observed a modest decrease in GIRK currents elicited by the GIRK channel activator ML297 in SAN cells from *Rgs6*$^{-/-}$ mice. Thus, RGS6 may facilitate efficient GIRK channel signaling in SAN cells, perhaps via physical interaction (42). The increase in A_1R-GIRK channel signaling seen with *Rgs6* ablation, however, suggests that this is not the main influence of RGS6 in SAN cells. Other work has called attention to the role of adaptor proteins, including R7BP and GPR158, in fine-tuning the influence of RGS proteins (21, 43–45). While R7BP or GPR158 expression has not been observed in the heart (46, 47), an unknown adaptor protein(s) may influence the impact of RGS6/Gβ5 on GIRK-dependent signaling in cardiomyocytes.

Previous work has implicated $G\alpha_o$ in the bradycardic effects of A_1R and M_2R activation. For example, isolated hearts from mice with a global knockout of $G\alpha_o$, but not of $G\alpha_{i2}$ or $G\alpha_{i3}$, exhibited diminished CCh-induced bradycardia (33). Additionally, work with embryonic stem cell-derived cardiomyocytes (ESDCs) showed that the reduction in isoproterenol-stimulated beating rate elicited by M_2R and A_1R activation was exaggerated in cells containing an RGS-insensitive version of $G\alpha_o$ (48). Our findings that $G\alpha_o$ is a critical mediator of M_2R-GIRK signaling in mouse SAN cells, and that *Rgs6* ablation enhances both M_2R- and A_1R-mediated bradycardia, are in line with these reports. Interestingly, the enhanced A_1R-induced suppression of isoproterenol-stimulated beating rate seen in ESDCs harboring a RGS-insensitive $G\alpha_o$ mutant was not blunted by TTQ, suggesting that this effect of A_1R activation may not be GIRK-dependent (48). This contrasts with our finding that A_1R-mediated bradycardia is absent in *Girk4*$^{-/-}$ mouse hearts. These discrepancies likely arise from the different cell types and model systems employed, where the relative complements of GPCRs, G proteins, effectors, and RGS proteins may differ.

There is little consensus on relevance of $G\alpha_{i2}$ to HR regulation. Mice with a global deletion of $G\alpha_{i2}$ exhibited diminished CCh-induced bradycardia and resting tachycardia (31). Mice harboring an RGS-insensitive $G\alpha_{i2}$ displayed enhanced M_2R-induced bradycardia, and the enhanced effect of CCh on beating rate of ESDCs harboring this mutation was reversed by TTQ (48). These findings are consistent with a prominent role for $G\alpha_{i2}$ in mediating M_2R-GIRK signaling in SAN cells. However, atrial myocytes from mice lacking $G\alpha_{i2}$ exhibited increased CCh-induced GIRK responses, which was attributed to increased GIRK subunit expression (49). Moreover, mice lacking $G\alpha_{i2}$ selectively in the cardiac conduction system exhibited resting tachycardia but normal CCh-induced bradycardia (32). Thus, the impact of $G\alpha_{i2}$ ablation and RGS-insensitive $G\alpha_{i2}$ on CCh-induced bradycardia is model-dependent and may reflect an indirect (noncardiac) influence of $G\alpha_{i2}$ on HR regulation. Additionally, the impact of $G\alpha_{i2}$ on resting HR may be exerted through GIRK-independent mechanisms (50). For example, M_2R activation inhibits the hyperpolarization-activated channel (I_f) by suppressing adenylyl cyclase activity and cAMP production (3). Interestingly, M_2R-I_f coupling is more sensitive than M_2R-GIRK signaling in SAN cells (51). Our data show that $G\alpha_o$ plays a critical role in M_2R-GIRK signaling. This pathway is subject to negative regulation by RGS6 and therefore may be engaged only by strong parasympathetic activation. $G\alpha_{i2}$, which is less susceptible to the GAP activity of RGS6, may mediate M_2R-I_f coupling during periods of weaker parasympathetic activity.

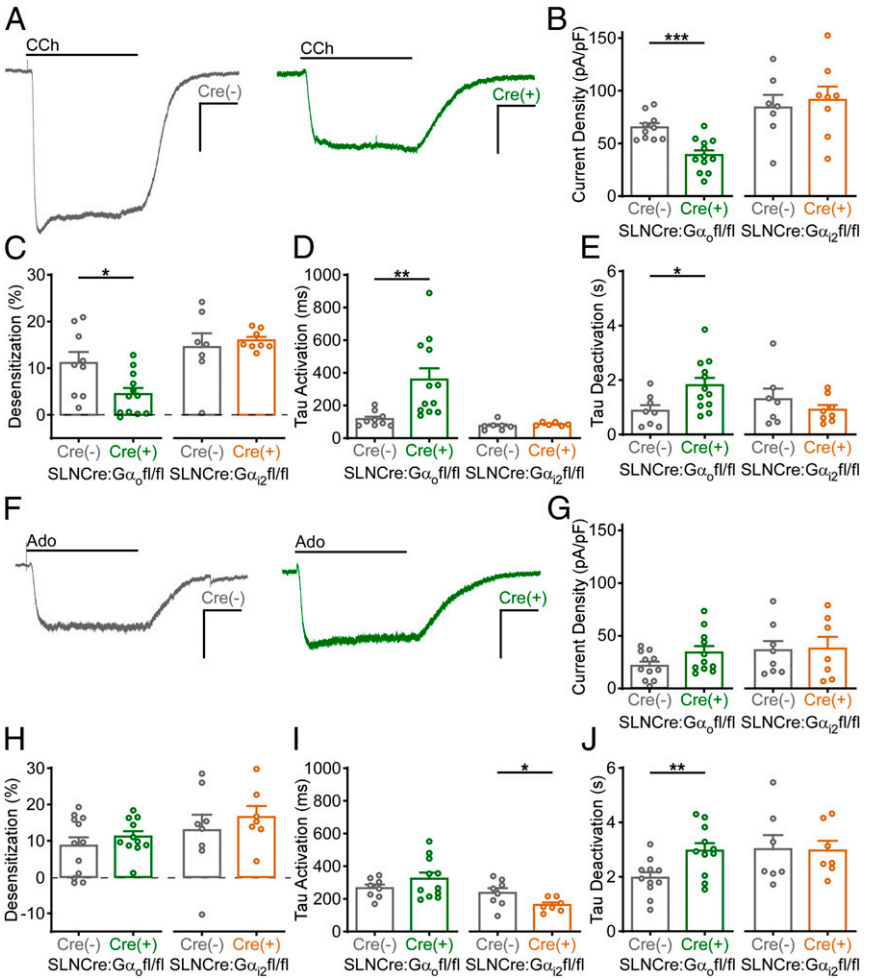

Fig. 7. Impact of $G\alpha_o$ and $G\alpha_{i2}$ ablation on CCh- and Ado-induced GIRK currents. (*A*) Whole-cell currents evoked by CCh (10 μM) in SAN cells from SLNCre(−):$G\alpha_o^{fl/fl}$ (*Left*, gray) and SLNCre(+):$G\alpha_o^{fl/fl}$ (*Right*, green) mice. (Scale bars: 5 s/500 pA.) (*B* and *C*) Peak CCh-induced current density ($t_{20} = 4.3$, ***$P < 0.001$; unpaired *t* test) and current desensitization ($t_{19} = 2.6$, *$P < 0.05$; unpaired *t* test) were smaller in SAN cells from SLNCre(+):$G\alpha_o^{fl/fl}$ mice as compared to their SLNCre(−):$G\alpha_o^{fl/fl}$ counterparts; group sizes ranged from 9 to 12 cells (5 mice) per genotype. There was no difference in CCh-induced current density ($t_{13} = 0.4$, $P = 0.69$; unpaired *t* test) or desensitization ($t_{13} = 0.5$, $P = 0.62$; unpaired *t* test) in SAN cells from SLNCre(−):$G\alpha_{i2}^{fl/fl}$ mice and SLNCre(+):$G\alpha_{i2}^{fl/fl}$ mice; group sizes ranged from 7 to 8 cells (3 mice) per genotype. (*D* and *E*) Activation ($t_{19} = 3.0$, **$P < 0.01$; unpaired *t* test) and deactivation ($t_{18} = 2.5$, *$P < 0.05$; unpaired *t* test) rates of CCh-induced currents were prolonged in SAN cells from SLNCre(+):$G\alpha_o^{fl/fl}$ mice, relative to SLNCre(−):$G\alpha_o^{fl/fl}$ counterparts; group sizes ranged from 8 to 12 cells (5 mice) per genotype. There was no difference in activation ($t_{11} = 0.9$, $P = 0.38$; unpaired *t* test) or deactivation ($t_{13} = 1.0$, $P = 0.36$; unpaired *t* test) rates of CCh-induced currents in SAN cells from SLNCre(−):$G\alpha_{i2}^{fl/fl}$ and SLNCre(+):$G\alpha_{i2}^{fl/fl}$ mice; group sizes ranged from 6 to 8 cells (3 mice) per genotype. (*F*) Whole-cell currents evoked by Ado (10 μM) in SAN cells from SLNCre(−):$G\alpha_o^{fl/fl}$ (*Left*, gray) and SLNCre(+):$G\alpha_o^{fl/fl}$ (*Right*, green) mice. (Scale bars: 5 s/500 pA.) (*G* and *H*) There was no difference in peak current density ($t_{20} = 1.8$, $P = 0.08$; unpaired *t* test) or desensitization ($t_{21} = 0.9$, $P = 0.38$; unpaired *t* test) of Ado-induced currents in SAN cells from SLNCre(−):$G\alpha_o^{fl/fl}$ and SLNCre(+):$G\alpha_o^{fl/fl}$ mice; group sizes ranged from 11 to 12 cells (4 mice) per genotype. There were no differences in Ado-induced current density ($t_{13} = 0.1$, $P = 0.91$; unpaired *t* test) or desensitization ($t_{13} = 0.7$, $P = 0.51$; unpaired *t* test) in SAN cells from SLNCre(−):$G\alpha_{i2}^{fl/fl}$ and SLNCre(+):$G\alpha_{i2}^{fl/fl}$ mice; group sizes ranged from 7 to 8 cells (3 mice) per genotype. (*I* and *J*) There was no difference in peak current density ($t_{20} = 1.8$, $P = 0.08$; unpaired *t* test) or desensitization ($t_{21} = 0.9$, $P = 0.38$; unpaired *t* test) of Ado-induced currents in SAN cells from SLNCre(−):$G\alpha_o^{fl/fl}$ and SLNCre(+):$G\alpha_o^{fl/fl}$ mice; group sizes ranged from 11 to 12 cells (4 mice) per genotype. There was an increase in activation rate ($t_{13} = 2.2$, *$P < 0.05$; unpaired *t* test) of Ado-induced currents in SAN cells from SLNCre(+):$G\alpha_{i2}^{fl/fl}$ mice as compared to SLNCre(−):$G\alpha_{i2}^{fl/fl}$ littermates. There was no difference in deactivation rate ($t_{12} = 0.08$, $P = 0.94$; unpaired *t* test) of Ado-induced currents in SAN cells from SLNCre(−):$G\alpha_{i2}^{fl/fl}$ and SLNCre(+):$G\alpha_{i2}^{fl/fl}$ mice; group sizes ranged from 7 to 8 cells (3 mice) per genotype.

It is important to recognize that genetic ablation of an individual Gα isoform redirects signaling to residual G protein isoforms. Ablation of $G\alpha_o$, for example, routes M_2R-GIRK signaling through $G\alpha_i$. In our hands, this yielded small CCh-induced GIRK currents with slow activation rates, reminiscent of Ado-induced GIRK currents in wild-type SAN cells. In contrast, routing A_1R-GIRK signaling through $G\alpha_i$ had no impact on Ado-induced current amplitude or activation kinetics. $G\alpha_o$ ablation did increase the sensitivity of GIRK channels to Ado, suggesting that (residual) $G\alpha_i$ is more efficient than $G\alpha_o$ at mediating A_1R-GIRK signaling in mouse SAN cells. Similarly, $G\alpha_{i2}$ ablation increased the sensitivity of GIRK channels to CCh, suggesting that (residual) $G\alpha_o$ is a more efficient mediator than $G\alpha_{i2}$ of M_2R-GIRK signaling in mouse SAN cells. The modest overall impact of $G\alpha_{i2}$ ablation, particularly on A_1R-GIRK signaling, is likely attributable to the presence of residual $G\alpha_{i1}$ and $G\alpha_{i3}$ isoforms (49). Indeed, this likely explains why there was no impact of global ablation of any single G-protein isoform ($G\alpha_o$, $G\alpha_{i2}$, $G\alpha_{i1/3}$) on GIRK-dependent bradycardia elicited by the A_1R agonist 2-chloro-N^6-cyclopentyladenosine (CCPA) (32).

Ado can provoke atrial fibrillation through shortening of the effective refractory period, an effect thought to be mediated by

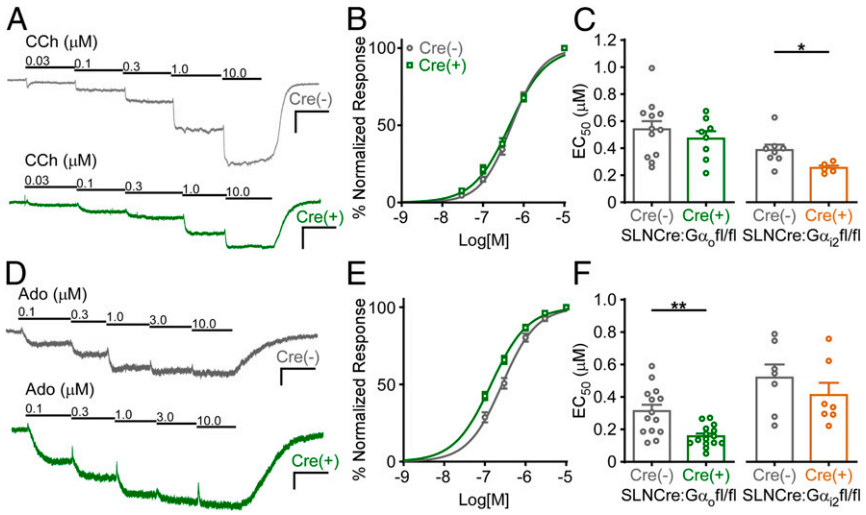

Fig. 8. Impact of $G\alpha_o$ or $G\alpha_{i2}$ ablation on GIRK channel sensitivity to CCh and Ado. (*A*) Concentration-response experiments of CCh-induced currents in SAN cells from SLNCre(–):$G\alpha_o^{fl/fl}$ (*Top*) and SLNCre(+):$G\alpha_o^{fl/fl}$ (*Bottom*) mice. (*B*) Summary of CCh sensitivity experiments in SAN cells from SLNCre(–):$G\alpha_o^{fl/fl}$ and SLNCre(+):$G\alpha_o^{fl/fl}$ mice. (*C*) There was no difference in EC_{50} values of CCh-induced GIRK currents in SAN cells from SLNCre(–):$G\alpha_o^{fl/fl}$ ($n = 12$ cells/3 mice) and SLNCre(+):$G\alpha_o^{fl/fl}$ ($n = 8$ cells/3 mice) mice ($t_{18} = 0.8$, $P = 0.44$; unpaired t test), but there was a decrease in the EC_{50} value in SAN cells from SLNCre(+):$G\alpha_{i2}^{fl/fl}$ ($n = 5$ cells/3 mice) compared to SLNCre(–):$G\alpha_{i2}^{fl/fl}$ ($n = 8$ cells/3 mice) mice ($t_{11} = 2.5$, $^*P < 0.05$; unpaired t test). (*D*) Concentration-response experiments of Ado-induced GIRK currents in SAN cells from SLNCre(–):$G\alpha_o^{fl/fl}$ (*Top*) and SLNCre(+):$G\alpha_o^{fl/fl}$ (*Bottom*) mice. (*E*) Summary of concentration-response experiments of Ado-induced GIRK currents in SAN cells from SLNCre(–):$G\alpha_o^{fl/fl}$ and SLNCre(+):$G\alpha_o^{fl/fl}$ mice. (*F*) The EC_{50} value for Ado-induced signaling in SAN cells from SLNCre(+):$G\alpha_o^{fl/fl}$ ($n = 15$ cells/3 mice) mice was lower than that measured in SAN cells from SLNCre(–):$G\alpha_o^{fl/fl}$ ($n = 12$ cells/3 mice) mice ($t_{25} = 3.3$, $^{**}P < 0.01$; unpaired t test), but there was no difference in EC_{50} value in SAN cells from SLNCre(–):$G\alpha_{i2}^{fl/fl}$ ($n = 7$ cells/3 mice) and SLNCre(+):$G\alpha_{i2}^{fl/fl}$ ($n = 7$ cells/3 mice) mice ($t_{12} = 1.0$, $P = 0.35$; unpaired t test).

GIRK channel activation in atrial myocytes (14). Enhanced A_1R and GIRK channel expression are associated with increased bradycardia in a tachypacing-induced chronic heart failure model in dogs (52). Moreover, atrial fibrillation induced by A_1R activation or M_2R activation (via vagal nerve stimulation) is thought to be mediated in part by GIRK channel activity (53, 54). While loss of GIRK4 in mice conferred resistance to pacing-induced atrial fibrillation (55), *Rgs6* ablation resulted in a higher incidence of atrial fibrillation induction (26). Similar to the impact of *Girk4* ablation, peptides targeting specific $G\alpha_i$ isoforms reduced atrial fibrillation susceptibility during vagal nerve stimulation in dogs (56). These and related observations, together with our results, show that interventions that suppress the influence of inhibitory G-protein signaling in atria by targeting signaling mediators and regulators or effectors could prove beneficial for treatment of certain arrhythmias and heart failure.

Insights gained in this study are likely to be relevant to the compartmentalization of GPCR-dependent signaling in other cell types, including neurons. GIRK channel regulation by inhibitory GPCRs has been implicated in neurological disorders including epilepsy, pain and analgesia, anxiety and depression, and addiction (57, 58). Neuronal GIRK-dependent signaling pathways regulated by $GABA_BR$, $5\text{-}HT_{1A}R$, and A_1R exhibit distinct amplitude and kinetic profiles and are differentially susceptible to plasticity (59–62). Our previous work has highlighted the integral role of RGS7, another member of the R7 RGS family, in modulating the kinetics and sensitivity of $GABA_BR$-GIRK signaling in hippocampal neurons (42, 43, 63, 64). Furthermore, RGS7 prefers $G\alpha_o$ over $G\alpha_i$ as a substrate for its GAP activity (28). Thus, GPCR-G protein and RGS-G protein substrate preferences likely shape neuronal GPCR-GIRK signaling dynamics in neurons and may help the functional compartmentalization of these signaling pathways.

Materials and Methods

Animals. All procedures involving mice were approved by the Institutional Animal Care and Use Committee of the University of Minnesota, and experiments were conducted in accordance with guidelines set by the NIH. The generation of *Girk4*$^{-/-}$ and *Rgs6*$^{-/-}$ mice was described previously (10, 19). C57BL/6J mice, bred on site or purchased from The Jackson Laboratory, were used as wild-type controls for these studies. Mice lacking either $G\alpha_o$ or $G\alpha_{i2}$ selectively in atrial/SAN tissue were generated by crossing the SLNCre driver mouse line (34) with floxed versions of either $G\alpha_o$ (35) or $G\alpha_{i2}$ (32), resulting in SLNCre:$G\alpha_o^{fl/fl}$ and SLNCre:$G\alpha_{i2}^{fl/fl}$ mouse lines, respectively. Male and female mice were group-housed on a 12-h light/dark cycle, given free access to food and water, and used for experiments at ages 8 to 12 wk.

SAN Cell Culture and Recordings. SAN cells were prepared for electrophysiological analysis as described (40). See *SI Appendix* for further details.

Isolated Heart Recordings. Hearts were excised and placed into ice-cold, oxygenated Tyrode's solution, and the aorta was quickly cannulated. Cannulated hearts were then placed into a warm (37 ± 1 °C) Tyrode's bath, and iWorx platinum recording electrodes were placed near/on the surface of the heart. Oxygenated Tyrode's solution was then perfused at 2 to 3 mL/min, and a baseline HR was recorded. Increasing concentrations of CCh or CPA (Tocris Bioscience) were then perfused via peristaltic pump for at least 15 min per dose. The electrocardiogram (ECG) signal was acquired with LabScribe v.3 software (iWorx) and filtered as appropriate. The derivative of that channel was computed to account for movements in baseline and to amplify the signal for subsequent analysis. A 30-s segment from the last minute of exposure to each agonist dose was then exported to Kubios HRV v.2 (65) for HR analysis, utilizing artifact correction as appropriate.

Quantitative RT-PCR. Total RNA was isolated from freshly isolated atrial tissue samples from adult wild-type mice and *Rgs6*$^{-/-}$ mice using the RNeasy fibrous tissue kit (Qiagen), according to manufacturer recommendations. Reverse transcription of 1.2 μg of total RNA per sample was performed using Maxima H Minus First Strand cDNA Synthesis Kit (ThermoFisher Scientific). Quantitative PCR was performed in a QuantStudio3 Real Time PCR System (Applied Biosystems) with the Fast SYBR Green Master Mix (ThermoFisher Scientific). See *SI Appendix* for further details, including target-specific primer sequences, reaction conditions, and analysis information.

Fast Kinetic BRET Assay. HEK293T/17 cells were grown in Dulbecco's Modified Eagle Media (Thermo Fisher Scientific) supplemented with 10% fetal bovine serum (Millipore Sigma), minimum Eagle's medium nonessential amino acids, 1 mM sodium pyruvate, and antibiotics (100 units/mL penicillin and

100 mg/mL streptomycin) at 37 °C in a humidified incubator containing 5% CO_2. Culture dishes (3.5 cm) were incubated for 10 min at 37 °C with 1 mL of 10 mg/mL growth-factor–reduced Matrigel (BD Biosciences) in culture medium. For transfection, cells were seeded into 3.5-cm dishes at a density of 2×10^6 cells/dish. After 2 h, expression constructs (total 5 μg/dish) were added to the cells using PLUS (5 μg/dish) and Lipofectamine LTX (6 μL/dish) reagents (Thermo Fisher Scientific). BRET measurements of Venus-Gβ1γ2 and masGRK3ct-Nluc-HA were performed to measure G protein activation by M_2R and A_1R, or the GAP activity of RGS6/Gβ5 in living cells, as described (27, 66). See *SI Appendix* for further details, including information about DNA constructs and transfection as well as BRET assay procedures and analysis.

Statistical Analysis. All data were analyzed using Prism v.8.2.1 software (GraphPad Software) and are presented as mean ± SEM. Statistical outliers were identified and excluded with Grubb's outlier test. The level of statistical significance was set at $P < 0.05$. Specific statistical analyses are denoted within the figure legends.

Data Availability. All experimental procedures and data supporting the findings of this paper are included in the article and *SI Appendix*. Requests for reagents used in this study should be directed to K.W.

ACKNOWLEDGMENTS. We thank Dr. C. David Weaver and Dr. Corey Hopkins for providing ML297, Nickolas Skamangas for technical support, and Hannah Oberle and Mehrsa Zahiremami for exceptional care of the mouse colony. This work was supported by NIH Grants HL105550 (to K.W. and K.A.M.), R21 HL124503 (to A.N.), and F31 HL139090 (A.A.) and by NIH Intramural Research Program Project Grant Z01-ES-101643 (to L.B.).

1. A. S. Hauser, M. M. Attwood, M. Rask-Andersen, H. B. Schiöth, D. E. Gloriam, Trends in GPCR drug discovery: New agents, targets and indications. *Nat. Rev. Drug Discov.* **16**, 829–842 (2017).
2. J. Dyavanapalli, O. Dergacheva, X. Wang, D. Mendelowitz, Parasympathetic vagal control of cardiac function. *Curr. Hypertens. Rep.* **18**, 22 (2016).
3. S. Dhein, C. J. van Koppen, O. E. Brodde, Muscarinic receptors in the mammalian heart. *Pharmacol. Res.* **44**, 161–182 (2001).
4. B. Sakmann, A. Noma, W. Trautwein, Acetylcholine activation of single muscarinic K^+ channels in isolated pacemaker cells of the mammalian heart. *Nature* **303**, 250–253 (1983).
5. D. E. Logothetis, Y. Kurachi, J. Galper, E. J. Neer, D. E. Clapham, The β γ subunits of GTP-binding proteins activate the muscarinic K^+ channel in heart. *Nature* **325**, 321–326 (1987).
6. K. D. Wickman *et al*., Recombinant G-protein β γ-subunits activate the muscarinic-gated atrial potassium channel. *Nature* **368**, 255–257 (1994).
7. S. Corey, D. E. Clapham, Identification of native atrial G-protein-regulated inwardly rectifying K^+ (GIRK4) channel homomultimers. *J. Biol. Chem.* **273**, 27499–27504 (1998).
8. S. Corey, G. Krapivinsky, L. Krapivinsky, D. E. Clapham, Number and stoichiometry of subunits in the native atrial G-protein-gated K^+ channel, I_{KACh}. *J. Biol. Chem.* **273**, 5271–5278 (1998).
9. G. Krapivinsky *et al*., The G-protein-gated atrial K^+ channel I_{KACh} is a heteromultimer of two inwardly rectifying K(+)-channel proteins. *Nature* **374**, 135–141 (1995).
10. K. Wickman, J. Nemec, S. J. Gendler, D. E. Clapham, Abnormal heart rate regulation in GIRK4 knockout mice. *Neuron* **20**, 103–114 (1998).
11. I. Bettahi, C. L. Marker, M. I. Roman, K. Wickman, Contribution of the Kir3.1 subunit to the muscarinic-gated atrial potassium channel I_{KACh}. *J. Biol. Chem.* **277**, 48282–48288 (2002).
12. P. Mesirca *et al*., The G-protein-gated K^+ channel, I_{KACh}, is required for regulation of pacemaker activity and recovery of resting heart rate after sympathetic stimulation. *J. Gen. Physiol.* **142**, 113–126 (2013).
13. S. W. Lee *et al*., Atrial GIRK channels mediate the effects of vagus nerve stimulation on heart rate dynamics and arrhythmogenesis. *Front. Physiol.* **9**, 943 (2018).
14. J. Layland, D. Carrick, M. Lee, K. Oldroyd, C. Berry, Adenosine: Physiology, pharmacology, and clinical applications. *JACC Cardiovasc. Interv.* **7**, 581–591 (2014).
15. S. J. Mustafa, R. R. Morrison, B. Teng, A. Pelleg, Adenosine receptors and the heart: Role in regulation of coronary blood flow and cardiac electrophysiology. *Handb. Exp. Pharmacol.* **193**, 161–188 (2009).
16. L. Belardinelli, W. R. Giles, A. West, Ionic mechanisms of adenosine actions in pacemaker cells from rabbit heart. *J. Physiol.* **405**, 615–633 (1988).
17. G. E. Woodard, I. Jardín, A. Berna-Erro, G. M. Salido, J. A. Rosado, Regulators of G-protein-signaling proteins: Negative modulators of G-protein-coupled receptor signaling. *Int. Rev. Cell Mol. Biol.* **317**, 97–183 (2015).
18. E. Posokhova, N. Wydeven, K. L. Allen, K. Wickman, K. A. Martemyanov, RGS6/Gβ5 complex accelerates I_{KACh} gating kinetics in atrial myocytes and modulates parasympathetic regulation of heart rate. *Circ. Res.* **107**, 1350–1354 (2010).
19. N. Wydeven, E. Posokhova, Z. Xia, K. A. Martemyanov, K. Wickman, RGS6, but not RGS4, is the dominant regulator of G protein signaling (RGS) modulator of the parasympathetic regulation of mouse heart rate. *J. Biol. Chem.* **289**, 2440–2449 (2014).
20. J. Yang *et al*., RGS6, a modulator of parasympathetic activation in heart. *Circ. Res.* **107**, 1345–1349 (2010).
21. G. R. Anderson, E. Posokhova, K. A. Martemyanov, The R7 RGS protein family: Multisubunit regulators of neuronal G protein signaling. *Cell Biochem. Biophys.* **54**, 33–46 (2009).
22. W. Jin, A. M. Klem, J. H. Lewis, Z. Lu, Mechanisms of inward-rectifier K^+ channel inhibition by tertiapin-Q. *Biochemistry* **38**, 14294–14301 (1999).
23. W. Jin, Z. Lu, Synthesis of a stable form of tertiapin: A high-affinity inhibitor for inward-rectifier K^+ channels. *Biochemistry* **38**, 14286–14293 (1999).
24. K. Kaufmann *et al*., ML297 (VU0456810), the first potent and selective activator of the GIRK potassium channel, displays antiepileptic properties in mice. *ACS Chem. Neurosci.* **4**, 1278–1286 (2013).
25. N. Wydeven *et al*., Mechanisms underlying the activation of G-protein-gated inwardly rectifying K^+ (GIRK) channels by the novel anxiolytic drug, ML297. *Proc. Natl. Acad. Sci. U.S.A.* **111**, 10755–10760 (2014).
26. E. Posokhova *et al*., Essential role of the m2R-RGS6-I_{KACh} pathway in controlling intrinsic heart rate variability. *PLoS One* **8**, e76973 (2013).
27. I. Masuho *et al*., Distinct profiles of functional discrimination among G proteins determine the actions of G protein-coupled receptors. *Sci. Signal.* **8**, ra123 (2015).
28. I. Masuho, K. Xie, K. A. Martemyanov, Macromolecular composition dictates receptor and G protein selectivity of regulator of G protein signaling (RGS) 7 and 9-2 protein complexes in living cells. *J. Biol. Chem.* **288**, 25129–25142 (2013).
29. G. J. Digby, P. R. Sethi, N. A. Lambert, Differential dissociation of G protein heterotrimers. *J. Physiol.* **586**, 3325–3335 (2008).
30. S. B. Hooks *et al*., RGS6, RGS7, RGS9, and RGS11 stimulate GTPase activity of Gi family G-proteins with differential selectivity and maximal activity. *J. Biol. Chem.* **278**, 10087–10093 (2003).
31. Z. Zuberi, L. Birnbaumer, A. Tinker, The role of inhibitory heterotrimeric G proteins in the control of in vivo heart rate dynamics. *Am. J. Physiol. Regul. Integr. Comp. Physiol.* **295**, R1822–R1830 (2008).
32. S. Sebastian *et al*., The in vivo regulation of heart rate in the murine sinoatrial node by stimulatory and inhibitory heterotrimeric G proteins. *Am. J. Physiol. Regul. Integr. Comp. Physiol.* **305**, R435–R442 (2013).
33. S. Z. Duan, M. Christe, D. S. Milstone, R. M. Mortensen, Go but not Gi2 or Gi3 is required for muscarinic regulation of heart rate and heart rate variability in mice. *Biochem. Biophys. Res. Commun.* **357**, 139–143 (2007).
34. H. Nakano *et al*., Cardiac origin of smooth muscle cells in the inflow tract. *J. Mol. Cell. Cardiol.* **50**, 337–345 (2011).
35. R. Ang, J. Abramowitz, L. Birnbaumer, A. V. Gourine, A. Tinker, The role of GαO-mediated signaling in the rostral ventrolateral medulla oblongata in cardiovascular reflexes and control of cardiac ventricular excitability. *Physiol. Rep.* **4**, e12860 (2016).
36. H. Cho, Regulation of adenosine-activated GIRK channels by Gq-coupled receptors in mouse atrial myocytes. *Korean J. Physiol. Pharmacol.* **14**, 145–150 (2010).
37. M. Bünemann, L. Pott, Down-regulation of A1 adenosine receptors coupled to muscarinic K+ current in cultured Guinea-pig atrial myocytes. *J. Physiol.* **482**, 81–92 (1995).
38. M. C. Wellner-Kienitz, K. Bender, T. Meyer, M. Bünemann, L. Pott, Overexpressed A(1) adenosine receptors reduce activation of acetylcholine-sensitive $K^{(+)}$ current by native muscarinic M(2) receptors in rat atrial myocytes. *Circ. Res.* **86**, 643–648 (2000).
39. M.-C. Kienitz, C. Littwitz, K. Bender, L. Pott, Remodeling of inward rectifying $K^{(+)}$ currents in rat atrial myocytes by overexpression of A(1)-adenosine receptors. *Basic Res. Cardiol.* **106**, 953–966 (2011).
40. A. Anderson *et al*., Expression and relevance of the G protein-gated K^+ channel in the mouse ventricle. *Sci. Rep.* **8**, 1192 (2018).
41. K. B. McPherson *et al*., Regulators of G-protein signaling (RGS) proteins promote receptor coupling to G-protein-coupled inwardly rectifying potassium (GIRK) channels. *J. Neurosci.* **38**, 8737–8744 (2018).
42. K. Xie *et al*., Gbeta5 recruits R7 RGS proteins to GIRK channels to regulate the timing of neuronal inhibitory signaling. *Nat. Neurosci.* **13**, 661–663 (2010).
43. O. I. Ostrovskaya *et al*., Inhibitory signaling to ion channels in hippocampal neurons is differentially regulated by alternative macromolecular complexes of RGS7. *J. Neurosci.* **38**, 10002–10015 (2018).
44. M. Jayaraman, H. Zhou, L. Jia, M. D. Cain, K. J. Blumer, R9AP and R7BP: Traffic cops for the RGS7 family in phototransduction and neuronal GPCR signaling. *Trends Pharmacol. Sci.* **30**, 17–24 (2009).
45. C. Orlandi *et al*., Orphan receptor GPR158 is an allosteric modulator of RGS7 catalytic activity with an essential role in dictating its expression and localization in the brain. *J. Biol. Chem.* **290**, 13622–13639 (2015).
46. D. Grabowska *et al*., Postnatal induction and localization of R7BP, a membrane-anchoring protein for regulator of G protein signaling 7 family-Gbeta5 complexes in brain. *Neuroscience* **151**, 969–982 (2008).
47. C. Orlandi *et al*., GPR158/179 regulate G protein signaling by controlling localization and activity of the RGS7 complexes. *J. Cell Biol.* **197**, 711–719 (2012).
48. Y. Fu *et al*., Endogenous RGS proteins and Galpha subtypes differentially control muscarinic and adenosine-mediated chronotropic effects. *Circ. Res.* **98**, 659–666 (2006).
49. M. Nobles, D. Montaigne, S. Sebastian, L. Birnbaumer, A. Tinker, Differential effects of inhibitory G protein isoforms on G protein-gated inwardly rectifying K^+ currents in adult murine atria. *Am. J. Physiol. Cell Physiol.* **314**, C616–C626 (2018).
50. C. Ye, M. O. Sowell, P. M. Vassilev, D. S. Milstone, R. M. Mortensen, Galpha(i2), Galpha(i3)and Galpha(o) are all required for normal muscarinic inhibition of the cardiac calcium channels in nodal/atrial-like cultured cardiocytes. *J. Mol. Cell. Cardiol.* **31**, 1771–1781 (1999).
51. D. DiFrancesco, P. Ducouret, R. B. Robinson, Muscarinic modulation of cardiac rate at low acetylcholine concentrations. *Science* **243**, 669–671 (1989).

52. V. P. Long III *et al*., Chronic heart failure increases negative chronotropic effects of adenosine in canine sinoatrial cells via A1R stimulation and GIRK-mediated I_{Kado}. *Life Sci.* **240**, 117068 (2020).
53. N. Hashimoto, T. Yamashita, N. Tsuruzoe, Tertiapin, a selective IKACh blocker, terminates atrial fibrillation with selective atrial effective refractory period prolongation. *Pharmacol. Res.* **54**, 136–141 (2006).
54. N. Li *et al*., Adenosine-induced atrial fibrillation: Localized reentrant drivers in lateral right atria due to heterogeneous expression of adenosine A1 receptors and GIRK4 subunits in the human heart. *Circulation* **134**, 486–498 (2016).
55. P. Kovoor *et al*., Evaluation of the role of I(KACh) in atrial fibrillation using a mouse knockout model. *J. Am. Coll. Cardiol.* **37**, 2136–2143 (2001).
56. G. L. Aistrup *et al*., Targeted G-protein inhibition as a novel approach to decrease vagal atrial fibrillation by selective parasympathetic attenuation. *Cardiovasc. Res.* **83**, 481–492 (2009).
57. C. Lüscher, P. A. Slesinger, Emerging roles for G protein-gated inwardly rectifying potassium (GIRK) channels in health and disease. *Nat. Rev. Neurosci.* **11**, 301–315 (2010).
58. R. Luján, E. Marron Fernandez de Velasco, C. Aguado, K. Wickman, New insights into the therapeutic potential of Girk channels. *Trends Neurosci.* **37**, 20–29 (2014).
59. J. L. Leaney, Contribution of Kir3.1, Kir3.2A and Kir3.2C subunits to native G protein-gated inwardly rectifying potassium currents in cultured hippocampal neurons. *Eur. J. Neurosci.* **18**, 2110–2118 (2003).
60. H. J. Chung *et al*., G protein-activated inwardly rectifying potassium channels mediate depotentiation of long-term potentiation. *Proc. Natl. Acad. Sci. U.S.A.* **106**, 635–640 (2009).
61. R. Nassirpour *et al*., Morphine- and CaMKII-dependent enhancement of GIRK channel signaling in hippocampal neurons. *J. Neurosci.* **30**, 13419–13430 (2010).
62. E. Marron Fernandez de Velasco *et al*., GIRK2 splice variants and neuronal G protein-gated K^+ channels: Implications for channel function and behavior. *Sci. Rep.* **7**, 1639 (2017).
63. O. Ostrovskaya *et al*., RGS7/Gβ5/R7BP complex regulates synaptic plasticity and memory by modulating hippocampal GABABR-GIRK signaling. *eLife* **3**, e02053 (2014).
64. A. Fajardo-Serrano *et al*., Association of Rgs7/Gβ5 complexes with Girk channels and GABAB receptors in hippocampal CA1 pyramidal neurons. *Hippocampus* **23**, 1231–1245 (2013).
65. M. P. Tarvainen, J.-P. Niskanen, J. A. Lipponen, P. O. Ranta-Aho, P. A. Karjalainen, Kubios HRV: Heart rate variability analysis software. *Comput. Methods Programs Biomed.* **113**, 210–220 (2014).
66. I. Masuho, K. A. Martemyanov, N. A. Lambert, Monitoring G protein activation in cells with BRET. *Methods Mol. Biol.* **1335**, 107–113 (2015).